World Academy of Science, Engineering and Technology
International Journal of Geological and Environmental Engineering
Vol:12, No:6, 2018

A Low-Power Two-Stage Seismic Sensor Scheme for Earthquake Early Warning System

Arvind Srivastav, Tarun Kanti Bhattacharyya

***Abstract*—**The north-eastern, Himalayan, and Eastern Ghats Belt of India comprise of earthquake-prone, remote, and hilly terrains. Earthquakes have caused enormous damages in these regions in the past. A wireless sensor network based earthquake early warning system (EEWS) is being developed to mitigate the damages caused by earthquakes. It consists of sensor nodes, distributed over the region, that perform majority voting of the output of the seismic sensors in the vicinity, and relay a message to a base station to alert the residents when an earthquake is detected. At the heart of the EEWS is a low-power two-stage seismic sensor that continuously tracks seismic events from incoming three-axis accelerometer signal at the first-stage, and, in the presence of a seismic event, triggers the second-stage P-wave detector that detects the onset of P-wave in an earthquake event. The parameters of the P-wave detector have been optimized for minimizing detection time and maximizing the accuracy of detection. Working of the sensor scheme has been verified with seven earthquakes data retrieved from IRIS. In all test cases, the scheme detected the onset of P-wave accurately. Also, it has been established that the P-wave onset detection time reduces linearly with the sampling rate. It has been verified with test data; the detection time for data sampled at 10Hz was around 2 seconds which reduced to 0.3 second for the data sampled at 100Hz.

***Keywords*—**Earthquake early warning system, EEWS, STA/LTA, polarization, wavelet, event detector, P-wave detector.

I. Introduction

THE Indian subcontinent is very susceptible to earthquakes: more than half of the area of India is considered earthquake-prone zone [1]. The north-eastern, Himalayan and Eastern Ghats Belts are the most vulnerable regions, where several earthquakes have caused enormous damages in the past. The 2011 Sikkim earthquake [2] of magnitude 6.9 and 2015 Gorkha, Nepal earthquake of magnitude 7.8 [3] killed thousands of people and caused property damages in tens of billions of dollars. A major factor behind occurrence of these earthquakes is the movement of Indian plate towards Eurasian plate at the rate of 47mm/year. The people and properties in the earthquake-prone regions are very vulnerable because the earthquakes cannot be predicted in advance. However, their arrival can be detected as a low-intensity faster moving primary wave (P-wave) comes a few seconds before the damaging secondary wave (S-wave). In these few seconds, an earthquake early warning system (EEWS) can alert the people that can significantly mitigate the potential damages. Many EEWSs have been deployed across the world. Some examples are UrEDAS (Urgent Earthquake Detection and Alarm System) in Japan [4], ElarmS (Earthquake Alarms Systems) [5] in California, USA, and PreSEIS (Pre-seismic Shaking) [6] in Istanbul, Turkey. The sensor nodes of these EEWSs monitor seismic activities in real-time and, in the wake of an earthquake event, alarm the people in the earthquake shake zone.

Arvind Srivastav and Tarun Kanti Bhattacharyya are with the Indian Institute of Technology, Kharagpur, WB 721302, India (e-mail: arvindsr@iitkgp.ac.in).

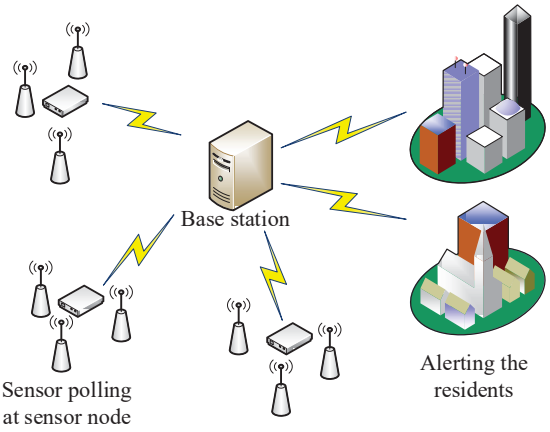

Fig. 1 The architecture of the EEWS wireless sensor network

A wireless sensor network based EEWS is being developed to be deployed in the earthquake-prone regions in India. It consists of wireless seismic sensors, distributed over the regions, that would detect the onset of the P-wave and transmit the data to nearest sensor node for majority voting based decision. The sensor node would communicate with the base station that would alert the residents in the earthquake shake zone. Fig. 1 shows the architecture of the EEWS sensor network.

The most important part of an EEWS is the seismic sensor that detects earthquakes in real-time. In the literature, several automated earthquake detection methods have been proposed. The STA/LTA (short-time-average over long-time-average trigger) algorithm [7] triggers by comparing the ratio of average in the longer moving window to shorter moving window with a defined threshold. Improvements of STA/LTA algorithm update LTA only in the quiet period [8], and calculate STA and LTA values in the moving window using L2 norm [9], instead of L1 norm used in the original algorithm. However, these algorithms rely on the statistics of the seismic signal; thus, they are prone to detecting non-earthquake seismic events as earthquake events and/or missing the detection of actual earthquake events.

P-wave detection algorithm uses polarization information of the seismic signal to detect the onset of P-wave [10]. The

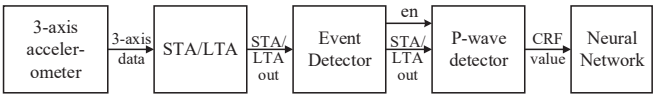

Fig. 2 Block diagram of the two-stage seismic sensor system

P-wave is longitudinally polarized from the hypocenter to the monitoring station which makes it distinctively different from other seismic signals. The P-wave detection algorithm performs eigenvalue decomposition of the seismic signal to extract the polarization information of the seismic signal. This method is more robust and accurate; however, it consumes a significant amount of power in doing the required computations. Learning based automated earthquake detection methods [11] are also coming up, which adjust weights for the features extracted to trigger at the onset of P-wave in the seismic signal even in a very noisy environment.

The P-wave detection method is robust, but a direct implementation is not feasible for our purpose. The seismic sensors would be deployed in the remote and hilly earthquake-prone terrains; therefore, these sensors need to be low-power devices. Thus, a robust and low-power two-stage earthquake detection scheme for the seismic sensors is being developed. The first stage comprises of STA/LTA and event detector blocks. The drifts and fluctuations present in the 3-axis accelerator signal are removed at STA/LTA block, and the seismic events are detected at the event detector block. When a seismic event is detected, the second stage, comprising of the P-wave detector and neural network blocks, is activated. At this stage, the P-wave detector block performs a wavelet-based multiresolution analysis (MRA) followed by windowing and singular value decomposition (SVD) on the incoming data. The generated output has a peak at the onset of the P-wave. This output is sent to a simple feed-forward neural network block for the final decision at the sensor. Fig. 2 shows the block diagram of the seismic sensor. The parameters of the P-wave detector have been optimized to minimize P-wave detection time and maximize the accuracy of detection. The P-wave detection scheme has been tested with seven test data from actual earthquakes retrieved from IRIS (Incorporated Research Institutions for Seismology). In all test cases, the seismic sensor accurately detected the arrival of P-waves. It has also been established that the P-wave detection time reduces linearly with increase in the sampling rate of the accelerometer signal. This finding has been verified with the test data; for test data sampled at 10Hz, the P-wave detection time was around 2 seconds, while for the test data sampled at 100Hz, the detection time was reduced to 0.3 second.

II. STA/LTA Block

Fig. 3 shows a 3-axis test data (test data #5, Table I). The three axes have very different biasing. In some cases, there is a substantial fluctuation in the biasing as well. These biasing and fluctuations influence the polarization information of the seismic signal which can lead to a very erroneous P-wave detection result. To remove biasing and fluctuations present, two moving windows—large and small—are formed at each axis to calculate long-time-sum (LTS) and short-time-sum (STS). The LTS and STS values are divided by the corresponding window size to result in LTA and STA values. The difference (= STA−LTA) is produced at the output for each axis.

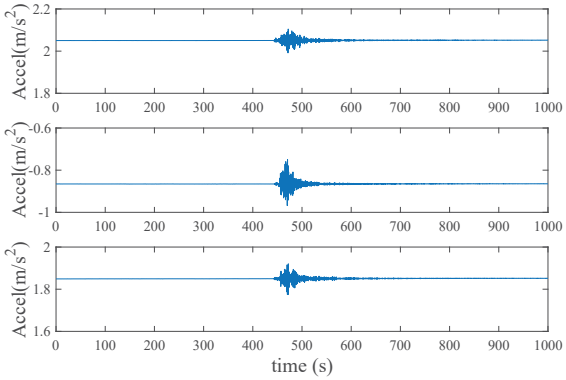

Fig. 3 Raw 3-axis data for test case #5

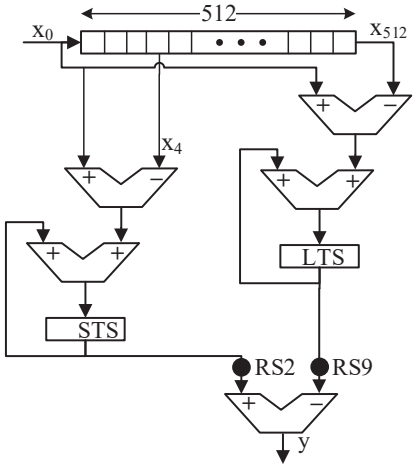

Fig. 4 Architecture of the STA/LTA block

A moving window of size 512 samples gave a fairly accurate estimation of the average value of the signal while a moving window of size 4 reduced the high-frequency noise without significantly compromising with the polarization information. Fig. 4 shows the architecture of the STA/LTA block. The 512 registers array stores past 512 samples for LTS calculation; the first four registers of this array are also for the STS calculation. Thus, for each new sample x_0, the LTS and STS values are modified as,

$$LTS = LTS + x_0 - x_{512} \quad (1)$$

$$STS = STS + x_0 - x_4 \quad (2)$$

The above equations give the update of the sum of all samples stored in the corresponding windows. To get the final output, the outputs of the LTS and STS registers are shifted by 9-bits and 2-bits respectively. Thus, the final output is,

$$y = \frac{STS}{4} - \frac{LTS}{512} \quad (3)$$

Initially, the registers are reset.

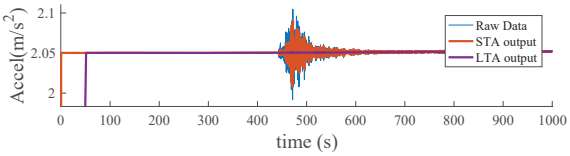

Fig. 5 Raw data, STA, and LTA plot for x-axis test data

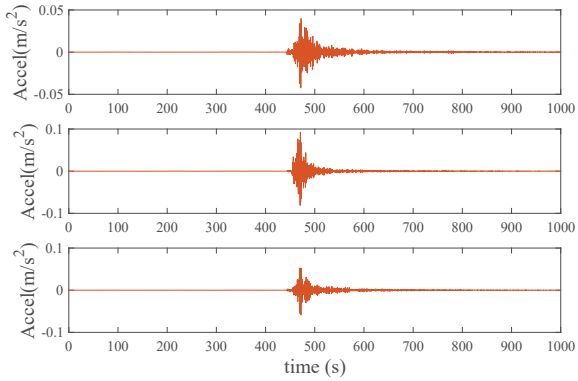

Fig. 6 STA/LTA block output for 3-axis seismic data

Fig. 5 plots the long-time average (LTA) and short-time average (STA) values on top of x-axis raw data of the test data #5.

Since the registers are reset in the beginning, the LTA computation takes 512 samples to give the correct values. Similarly, STA computation takes four samples. These are visible in Fig. 5 as the build-up of LTA and STA output waveforms. The STA/LTA block output of the 3-axis test data is shown in Fig. 6.

III. Event Detector

The P-wave detector at the second stage consumes a lot of power in performing the computations for extracting the polarization information of the seismic signal. Also, some unwanted peaks are present in the non-seismic activity zone of data (see Fig. 7) due to one or two axis value(s) being much larger in ratio compared to the rest (although all of them are close to zero at the LTA/STA output). Therefore, to remove unwanted spikes and minimize the power consumption, the second stage is activated only when a seismic event occurs. These seismic events are detected by forming moving windows of size N_E (= 24) on each axis of the STA/LTA output and finding the range of values ($MAX - min$) for each iteration in the windows. The maximum of the ranges of the three axes is compared with a threshold (thr) to detect the occurrence of the $events$ in real-time.

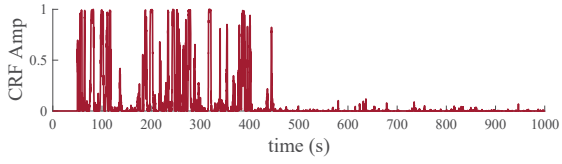

Fig. 7 P-wave detector output directly from STA/LTA data

Conventionally, a threshold-based event detection is used, which compares the input signal to a threshold for event detection. This method is simple in analog as well as digital implementation. However, for the test data set, it was observed that the non-seismic noise amplitude was comparable to the initial P-wave amplitude. Thus, the threshold-based event detection missed the onset of P-wave detection. On the other hand, the swing of the noise signal was much smaller in comparison to the P-wave amplitude. So, a more effective range-based event detection method was designed which ignored the non-seismic noise but picked the seismic events instantaneously. The algorithm for event detection is as follows:

$x_0 \leftarrow (input\ data)$
$x_N \leftarrow (window\ output\ data)$
$count \leftarrow 0$ $(event\ detector\ smoothing\ parameter)$
if $MAX = x_N$ **then**
  FINDMAX
else
  if $MAX < x_0$ **then**
    $MAX \leftarrow x_0$
  end if
end if
if $min = x_N$ **then**
  FINDMIN
else
  if $min > x_0$ **then**
    $min \leftarrow x_0$
  end if
end if
if $MAX - min > thr$ **then**
  $event = 1$
  $count \leftarrow 100$
else
  if $count > 0$ **then**
    $event = 1$
    $count = count - 1$
  else
    $event = 0$
  end if
end if

The algorithm introduces a parameter $count$ that smooths the event detector output to reduce toggles that add some unwanted peaks in the P-wave detector output. Based on testing, $N = 24$ and $thr = 10^{-3}$ is taken for the parameters. Since the statistics of the seismic signal recorded using the accelerometer of the seismic sensor may differ from that of the test data, that event detector algorithm may be modified in the hardware implementation.

Fig. 8 shows the event detector output plotted over the x-axis test data and the corresponding P-wave detector output.

IV. Wavelet-based P-Wave Detector

For an EEWS, it is very critical to accurately and reliably detect the onset of P-wave in real-time. The STA/LTA algorithm consumes very small power, but it cannot reliably differentiate earthquake signals from other seismic signals since it depends on the statistical properties of the seismic signal. This necessitates a more robust and accurate P-wave detection scheme for the seismic sensor. Kanasewich [10] developed a P-phase detection method that extracts the polarization information of the seismic signal to detect

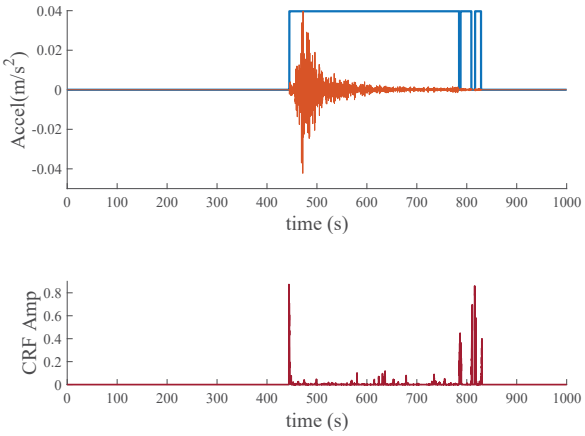

Fig. 8 Event detector output with count parameter (top) and corresponding CRF amplitude plot (bottom)

the onset of P-wave. This method performs multiresolution analysis to decompose the data at multiple wavelet scales, extracts polarization information at those scales, and multiplies them together to suppress the false results.

The P-wave detection scheme is as follows:

1) The incoming data (from STA/LTA block) is decomposed at different scales using multiresolution analysis (MRA). The Daubechies wavelet is used for the MRA as it closely resembles the earthquake waveform.
2) Moving windows of size N are formed at each level of the wavelet output for three axes to store the current data and past $N-1$ data.
3) Covariance matrix M defines as

$$M = \begin{bmatrix} Var(X) & Cov(X,Y) & Cov(X,Z) \\ Cov(Y,X) & Var(Y) & Cov(Y,Z) \\ Cov(Z,X) & Cov(Z,Y) & Var(Z) \end{bmatrix}$$

where,
Cov(X,Y) = $\sum_{i=1}^{N}(x_i - u_x)(y_i - u_y)$
and X,Y and Z are wavelet coefficients, is formed at all wavelet levels j.

4) Singular Value Decomposition (SVD) is applied to covariance matrices at each level to get the associated singular values. The covariance matrix M is multiplied with its Hermitian to extract the eigenvalues (λ_i's). Thus,

$$M = U\Sigma V \tag{4}$$

$$\Sigma^2 = M^H M = V^H \Sigma^2 V \tag{5}$$

where, Σ^2 is the diagonal eigenvalue matrix.

5) Rectilinearity function, F, defined as

$$F = 1 - \frac{\lambda_2}{\lambda_1} \tag{6}$$

where, λ_1 and λ_2 are largest and second largest eigenvalues from the SVD decomposition of covariance matrix, is calculated at each scale.

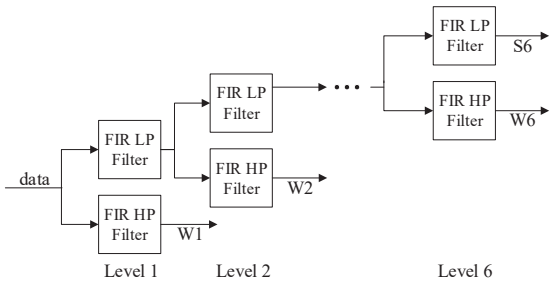

Fig. 9 Architecture of the multiresolution analysis. (S = scaled output, W = wavelet output)

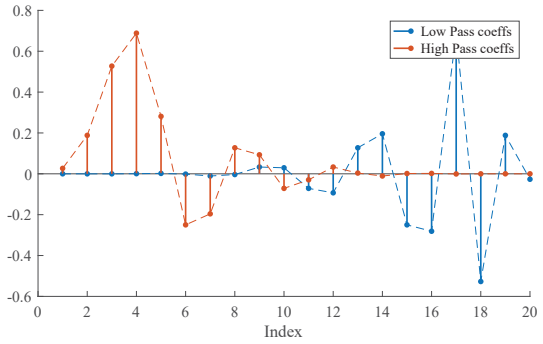

Fig. 10 The LP and HP filter coefficients for Daubechies 10 wavelet

6) The output of P-wave detector—composite rectilinearity function (CRF) is formed by multiplying F_j's at scales,

$$CRF = \prod_{j=1}^{L} F_j \tag{7}$$

7) CRF value ranges from 0 to 1 with the value close to zero value for unpolarized seismic data and near 1 for the polarized P-wave data.

The P-wave detection scheme has three parameters: wavelet number, wavelet levels (L), and window size (N). For the 10Hz test data, a cost minimization integer optimization script was used to minimize the root mean square (RMS) value of the CRF output in the non-seismic region, and maximize it in the P-wave region of test data. The parameters were swept in the range (2,12), (2,16), and (2,24), respectively. The optimum value achieved was Daubechies 10 wavelet, at six wavelet levels ($L = 6$), at window size of 12 ($N = 12$).

Fig. 9 shows the architecture of wavelet-based MRA. It has been implemented with a 16-bit fixed data point. Fig. 10 shows the discrete coefficients used for low-pass (LP) and high-pass (HP) finite impulse response (FIR) filters implementation. At each stage, the FIR HP filter generates the wavelet output while FIR LP filter generates the scaled data output.

After forming the moving windows at the MRA outputs, the SVD is implemented at each level using (4) and (5). The final CRF output is computed by multiplying the F_j's at each level, as described earlier.

V. Results

Table I lists onset of P-wave detection time for seven test data of recent earthquakes retried from IRIS. It has

TABLE I
ONSET OF P-WAVE DETECTION TIME FOR TEST DATA

No.	Loc.	Mag.	Date	Station	Sampling Rate	N	t_d
1	PNG	7.5	25/02/2018	PMG	10Hz	12	3.1s
2	PNG	7.5	25/02/2018	HNR	10Hz	12	1.4s
3	LL	7.6	25/12/2016	TRQA	10Hz	12	2.0s
4	LL	7.6	25/12/2016	LCO	10Hz	12	1.1s
5	GA	7.9	23/01/2018	COLA	10Hz	12	3.5s
6	GA	7.9	23/01/2018	KDAK	10Hz	12	1.7s
7	GA	7.9	23/01/2018	KDAK	100Hz	24	0.3s

(N = Window size; PNG = Papua New Guinea, New Guinea; LL = Los Lagos, Chile; GA = Gulf of Alaska, USA)

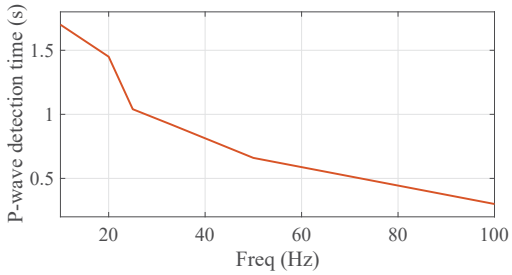

Fig. 11 P-wave detection time (in second) vs sampling rate (in Hz)

six 10Hz data and one 100Hz test data. Several 100Hz earthquake data were retrieved from IRIS, but all except one were fragmented. The seismic sensor scheme takes around 2 seconds for detecting the onset of P-wave for 10Hz sampled data while only 0.3 second for detecting the onset of P-wave for 100Hz sampled data. This linear reduction in detection time with increase in sampling frequency was predicted from the implementation of the scheme: The P-wave detection scheme needs a few more samples than the window size (N) to build the CRF peak at the onset of P-wave. As the window size does not increase significantly with increase in sampling rate, the required number of samples for CRF peak buildup are available in shorter duration for a higher sampling rate. This result has also been verified with the test data #7, sampled at 100Hz. Lower sampling rate test data (at $100/n$Hz) were generated by picking every n^{th} sample of the 100Hz test data. The P-wave detection scheme was ran at these test data and the corresponding P-wave detection time is plotted in Fig. 11. It can be seen that the detection time reduces linearly with increase in the sampling rate. However, it can be argued that this reduction will crease at a sampling frequency, as sampling the signal higher than that frequency will have samples taken from a small part of P-wave waveform, which would not capture the polarization information of the P-wave signal.

Two sample test cases and corresponding P-wave detector outputs are plotted in Fig. 12 (test case #2, sampling rate: 10Hz) and Fig. 13 (test case #7, sampling rate: 100Hz). It can be seen that the onset of P-wave is detected very effectively using the two-stage scheme. Some undesired CRF peaks are also present in the P-wave detector output. Thus, the event detector output along with the P-wave detector output would be sent to a trained neural network for final classification.

Table II compares the time taken by the P-wave detector system to the state-of-the-art in earthquake detection. The P-wave detector time is taken for 100Hz sampling test case,

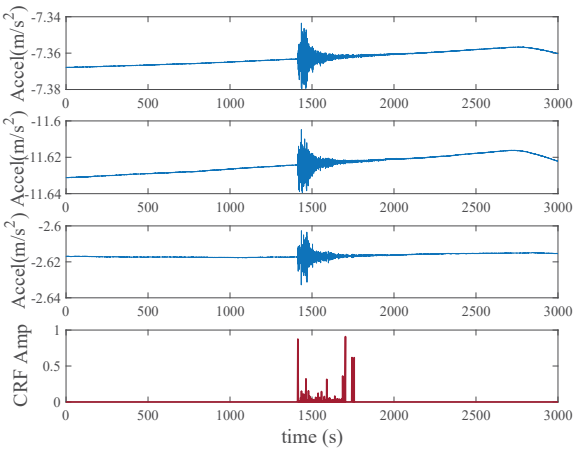

Fig. 12 The P-wave detector output plot for test case #2

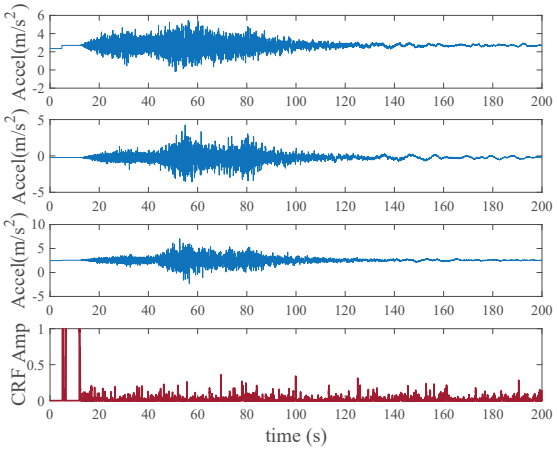

Fig. 13 The P-Wave Detector Output Plot for Test Case #7

TABLE II
COMPARISON WITH THE STATE-OF-THE-ART

No.	EEWS	Alerting/ P-wave detection time
1	UrEDAS [4]	3 sec
2	ElarmS [5]	5 sec
3	PreSEIS [6]	2 sec
4	Two-stage detector (100Hz)	0.3 sec

as the same sampling rate is being used for the hardware implementation. It should be noted that the state-of-the-art do not specifically mention the time required for P-wave detection; they instead mention the alert time from the onset of P-wave at their sensor network. Since the proposed scheme takes only a fraction of a second in detecting the onset of an earthquake, it is at par with the state-of-the-art in earthquake detection time.

VI. CONCLUSION AND FUTURE WORK

The P-wave detection scheme reliably and accurately detects the onset of P-wave. The P-wave detection time is very critical because the damaging S-wave is only a few seconds away, and in that time, the P-wave detector has to reliably

detect the onset of P-wave and communicate with the base station to send emergency warning messages on the phones, radio, and televisions of the residents in surrounding region. The residents can seek nearby shelter before an earthquake hits the area, which would reduce the damages. The P-wave detector system is being implemented at a sampling rate of 100Hz as the P-wave detection is almost real-time (only a fraction of a second) with this sampling rate. As the P-wave detector generates some undesired CRF peaks along with the actual peaks, the final decision is made at a feedforward neural network that classifies the results using the event detector and P-wave detector outputs. The developed scheme is currently being implemented on board level using ZedBoard in all digital fashion. After the verification of the working of the scheme in a simulated earthquake environment, a chip level implementation of the scheme would be carried out, wherein the first stage would be implemented in analog in the subthreshold region [12]. This would reduce the power consumption in event detection to orders of nW.

ACKNOWLEDGMENT

The authors would like to thank Professor Arun Singh and Professor Chandrani Singh, Department of Geology and Geophysics, IIT Kharagpur, and MeitY, Government of India for providing the support under the C2S program.

REFERENCES

[1] S. K. Jain, "Indian earthquakes : An overview," *The Indian Concrete Journal*, vol. 72, no. 11, 1998.

[2] D. Rai, G. Mondal, V. Singhal, N. Parool, and P. T., "2011 sikkim earthquake: Effects on building stocks and perspective on growing seismic risk," in *15th World Conference on Earthquake Engineering*, 2012.

[3] K. Goda, T. Kiyota, R. M. Pokhrel, G. Chiaro, T. Katagiri, K. Sharma, and S. Wilkinson, "The 2015 gorkha nepal earthquake: Insights from earthquake damage survey," *Frontiers in Built Environment*, vol. 1, p. 8, 2015. [Online]. Available: https://www.frontiersin.org/article/10.3389/fbuil.2015.00008

[4] Y. Nakamura, "Uredas, urgent earthquake detection and alarm system, now and future," in *13th World Conference on Earthquake Engineering*, 2004.

[5] A. R.M., "The elarms earthquake early warning methodology and its application across california," *Earthquake Early Warning Systems*, pp. 21–24, 2007.

[6] M. Böse, M. Erdik, and F. Wenzel1, *A New Approach to Earthquake Early Warning*. Berlin, Heidelberg: Springer Berlin Heidelberg, 2007, pp. 65–83.

[7] R. V. Allen, "Automatic earthquake recognition and timing from single traces," *Bulletin of the Seismological Society of America*, vol. 68, no. 5, p. 1521, 1978. [Online]. Available: + http://dx.doi.org/

[8] W. Jiang, H. Yu, L. Li, and L. Huang, "A robust algorithm for earthquake detector," in *15th World Conference on Earthquake Engineering*, 2012.

[9] M. Withers, R. Aster, C. Young, J. Beiriger, M. Harris, S. Moore, and J. Trujillo, "A comparison of select trigger algorithms for automated global seismic phase and event detection," *Bulletin of the Seismological Society of America*, vol. 88, no. 1, p. 95, 1998. [Online]. Available: + http://dx.doi.org/

[10] E. Kanasewich, *Time sequence analysis in geophysics. Third Ed., The University of Alberta Press, Alberta*. The University of Alberta Press, Alberta, 1981.

[11] R. R. Leach and F. U. Dowla, "Earthquake early warning system using real-time signal processing," in *Neural Networks for Signal Processing VI. Proceedings of the 1996 IEEE Signal Processing Society Workshop*, Sep 1996, pp. 463–472.

[12] U. Antao, A. Dibazar, J. Choma, and T. Berger, "Low power false positive tolerant event detector for seismic sensors," in *2013 IEEE SOI-3D-Subthreshold Microelectronics Technology Unified Conference (S3S)*, Oct 2013, pp. 1–2.